A Method to Realize Low Velocity Movability and Eliminate Friction Induced Noise in Piezoelectric Ultrasonic Motors

Bülent Delibas and Burhanettin Koc

***Abstract*—In a piezoelectric ultrasonic motor (USM) or resonance drive type piezoelectric motor (RPM), movement is generated between a vibrator (stator) and a slider (rotor). Since the microscopic vibrations on a stator are transferred to a slider through friction interaction, the movement of a slider has a nonlinear characteristic due to the nature of the friction force. This nonlinear behavior causes large position errors due to the occurrence of discontinuous stick-slip movements and unpleasant audible noise, especially at a low velocity drive. This friction induced acoustic sound is magnified at low velocities as the natural frequency of the mechanical system of a piezoelectric motor with mass and the holding and prestress spring forces are dependent on the closed loop motion controller. This article addresses the abovementioned issues. First, a mechanical model, which considers the nature of movements in a resonance drive type piezoelectric motor, was established. The model could suitably define the friction induced forced vibration and noise source. Second, a new driving method for resonance drive type piezoelectric motors was proposed, in which the piezoelectric vibrator was excited using two driving sources at two different frequencies. The difference between the two excitation frequencies was synchronized to the servo sampling frequency of the digital control unit. Finally, the performance of the proposed driving method was compared with those of the conventional driving methods. It was noted that in addition to the realization of silent and smooth low velocity movements, the positioning error for the linear movements between the desired and actual positions decreased to less than 10 nm for velocities ranging from 1 to 0.001 mm/s.**

***Index Terms*—Friction, motors, nonlinearities, piezoelectricity, position control.**

I. Introduction

PIEZOELECTRIC actuators and motors operate based on the inverse piezoelectric effect in which piezoelectric ceramic is electrically excited to generate a movement or strain [1]–[3]. An ultrasonic motor (USM) is a type of piezoelectric motor in which a high frequency oscillation is generated when the piezoelectric body is excited at resonance. With the technological advancements, these motors are being widely used in several industrial applications [4], [5]. Ultrasonic motors have attracted considerable attention, especially in the areas of micropositioning, photonics, biotechnology, and consumer electronics [6]–[8]. Ultrasonic motors can be designed and constructed using only a few parts in a compact volume, their energy consumption is low and their efficiency does not change considerably with the size. Furthermore, these motors can realize direct actuations without a gear assembly and are highly dynamic.

Since USMs are driven by means of a friction contact mechanism between a rotor and stator, a dead zone always exists between the speed and operating voltage. The operating voltage must be above a threshold voltage level to ensure that the pushing force generated by the microscopic vibration of the stator can exceed the breakaway friction force at the contact. Contact friction is a highly nonlinear phenomenon. Various friction models have been reported to describe the stiction and breakaway force at the interface of the USMs [9]–[11]. Furthermore, the dead zone is not direction symmetric, and its boundaries are unpredictable. The differences between the static and dynamic friction properties of the mating surfaces further enhance the nonlinearity and hysteresis of the voltage–speed characteristics [12], [13].

Huang *et al.* [14] recently presented a comprehensive review of the existing friction models with a detailed discussion regarding the intelligent control methods pertaining to both model based and model free compensation schemes in motion control systems. To enable high precision trajectory following for USMs, various sophisticated control concepts [14]–[24], such as model predictive control [15], fuzzy neural networks [21], adaptive backstepping [22] nonlinear PID [23], and sliding mode [24] have been investigated. However, precise motion at low velocities cannot be achieved using these advanced control methods [25], [26]. Precise smooth motion, especially at low velocities, is required for biomedical devices, robotic arms, microscopy stages and medical operations [27]. Moreover, noiseless actuation during the operation is a prerequisite for actuators, especially for military and consumer applications [28]. None of the abovementioned control methods provide a solution for the friction induced vibration or audible noises during the operation of a precision stage [29]–[31]. Therefore, a suitable driving method is needed to realize low velocity movability with friction induced noise suppression.

Manuscript received September 6, 2019; revised January 29, 2020; accepted March 17, 2020. Date of publication April 20, 2020; date of current version December 14, 2020. Recommended by Technical Editor Q. Xu. *(Corresponding author: Burhanettin Koc.)*

The authors are with the Physik Instrumente GmbH & Co. KG, 76228 Karlsruhe, Germany (e-mail: b.delibas@pi.ws; b.koc@pi.ws).

Color versions of one or more of the figures in this article are available online at http://ieeexplore.ieee.org.

Digital Object Identifier 10.1109/TMECH.2020.2984367

Pang *et al.* [32] investigated the dual frequency drive of a vibrator in a piezoelectric ultrasonic motor and proposed an analytical model describing the behavior of the friction tip under dual frequency actuation. In addition, Ming *et al.* [33] proposed an approach to realize the dual frequency drive on a different resonance drive type piezoelectric motor. However, in both these studies, the two frequencies applied to the vibrator were close to the main operating frequency of the vibrator; consequently, the slider movements in both the studies were not stable. In addition, no correlation was established between the servo loop control sampling frequency and actuation frequencies.

Takano *et al.* [34] addressed the problem of nonlinearity of the driving voltage and speed and proposed a solution to eliminate the dead zone nonlinearity, thereby improving the controllability at slow motion. In particular, the researchers used a multilayered piezoelectric stator element in which the normal and tangential components of the microscopic motion at the interface were generated independently by using the allocated driving electrodes.

In this article, a mechanical model, which describes the slow motion and friction induced vibration at the stator and slider interface for an ultrasonic motor, is introduced. This model takes into account the dependency of the slow motion and friction induced vibration to the motion parameters, such as acceleration, velocity, and geometric properties. Consequently, the use of this model provides a promising new driving method, which is effective, especially at low velocities. The proposed method uses two driving sources at two different frequencies, which excite the corresponding two eigenmodes of the piezoelectric vibrator. Such a driving technique can facilitate the position and velocity control of a resonance drive type piezoelectric motor. The acceleration generated by the stator at a high frequency is applied to the slider as the pushing force, and it can be controlled in each servo loop of a closed loop controller.

The rest of this article is organized as follows. Section II describes the motor structure and theory of motion for resonance drive type piezoelectric motors. Subsequently, a dual source dual frequency driving (DSDF) method is introduced. The performance evaluation of the new driving method is described in Section IV, and finally, Section V concludes this article.

II. Theory of Motion for Resonance Drive Type Piezoelectric Motors

A. Motor Structure

The vibrator of the ultrasonic motor considered in this study is a rectangular piezoelectric plate, and metallization electrodes are applied on its two main surfaces. While the electrodes on one surface cover the main surface completely, the electrodes on the other main surface divide the plate into two sections. A pusher is attached at the middle of one side surface [35]. The vibrator is manufactured by Physik Instrumente (PI) under the trade name of "PIline." To generate a movement, the vibrator must be held stationary and a prestress force should be applied against the mover. Therefore, as shown in Fig. 1, the vibrator is held stationary between a pivot point and a side spring. The

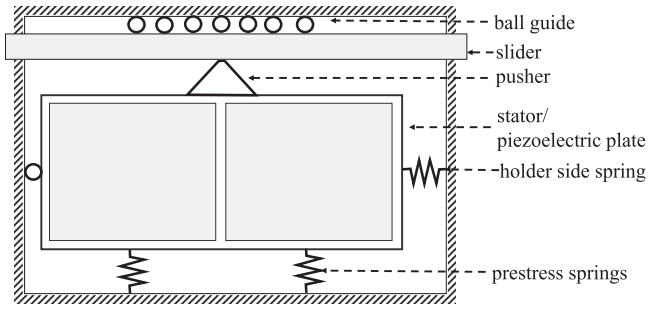

Fig. 1. Structure of a PILine motor integrated in the precision stage.

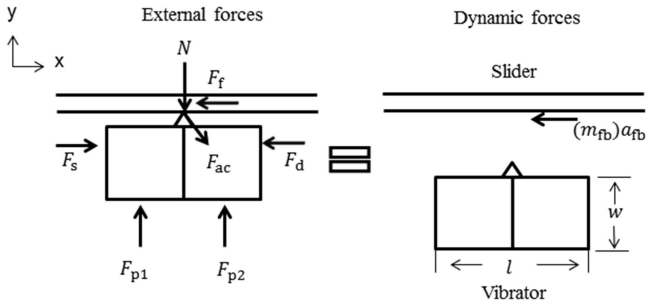

Fig. 2. Free body and kinetic diagram of the slider for a PILine motor.

prestress springs press the vibrator against the slider guided by a linear or rotary bearing.

To improve the precise movement, especially at low velocities, both the surface electrodes of the piezoelectric ceramic can be excited simultaneously to manipulate the pusher movements with two separate sources [38]. In the case of two source driving, both the magnitude and phase difference can be used as the control parameters. The driving concept is implemented precisely at the nonlinear region of friction; however, the motor efficiency deteriorates due to the higher voltages input to both the electrodes. Furthermore, the issue of acoustic noise at low velocities is not eliminated.

B. Force Acting on a Slider During Slow Motion

To understand the slow motion, the dynamic equations must be obtained using Newton's second law of motion. To apply the equation of motion, the free body and kinetic diagram of the vibrator and the slider including all the forces acting on these entities must be considered, as illustrated in Fig. 2. When one half of the vibrating piezoelectric plate is driven by an electrical signal, a planar (or radial) mode resonance frequency of the driven section is excited. The pusher and unexcited other half of the plate function as a perturbation mass. Consequently, an oblique motion at the tip of the pusher causes the sliding element to perform a linear movement.

As illustrated in Fig. 2, forces act on the sides of the vibrator body, and the pressing forces push the actuator to the slider owing to the pyramid shaped pusher. The forces acting in the y-axis direction, normal to the moving direction of the slider are

$$F_{\mathrm{p1}} + F_{\mathrm{p2}} - N - F_{\mathrm{acy}} = 0 \tag{1}$$

$$N = -F_{\mathrm{acy}} + 2F_p \tag{2}$$

where F_{p1} and F_{p2} denote the forces applied by the prestress springs, and N is the normal reaction force at the friction tip. F_{acx} and F_{acy} denote the vibrator actuation forces in the directions of the x and y axes, respectively. Since the movement of the friction tip is in the oblique direction, the force F_{ac}, which is generated by the vibrator, is oriented at approximately 45° to the x-axis. Therefore, F_{acx} and F_{acy} are assumed to be equivalent. Similarly, the forces acting in the x axis direction, which is the moving direction of the slider, can be expressed as in (3) and (4)

$$F_s - F_d - F_f + F_{acx} = 0 \tag{3}$$

$$F_{acx} = N\mu_s \tag{4}$$

where F_s and F_d denote the force applied by the holder spring from the side and the reaction force from the motor housing, respectively. F_f is the friction force at the tip of the vibrator, and μ_s is the static friction constant at the mating surface between the friction tip and the slider. Equations (1) and (2) correspond to the static case immediately before the slider starts to move. The pressing forces applied by the springs in the positive y-axis direction are assumed to be the same. In (1), $F_{p1} = F_{p2} = F_p$. Similarly, the holder spring force and reaction force from the housing in the x-axis direction are assumed to be equal, that is, $F_s = F_d$. In the dynamic case, immediately after the slider moves, the equation of motion and friction force can be expressed as in (5) and (6), respectively.

$$F_f = N\mu_d \tag{5}$$

$$-F_f + F_{acx} = m\,(a_{fb}) \tag{6}$$

where m is the moving mass including the slider, friction bar and carried load; and μ_d is the dynamic friction constant at the mating surface between the friction tip and the slider. By implementing (2)–(5) into (6), the acceleration of the slider can be determined as in (7).

$$a_{fb} = 2F_p\ (\mu_s - \mu_d) / ((1 + \mu_s)\, m) \tag{7}$$

Equation (7) states that, to obtain a small step, and thus a low velocity, the acceleration acting on the slider should also be small. Since the velocity and displacement of the slider can be calculated by integrating the acceleration as in (8) and (9), the aspect to be considered is how to reduce the acceleration and its duration during a small movement

$$v_{fb} = \int (a_{fb})\ dx \tag{8}$$

$$x_{fb} = \int (v_{fb}) dt \tag{9}$$

where v_{fb} and x_{fb} denote the velocity and movement of the slider, respectively.

The acceleration term must be as small as possible to ensure that the lowest velocity and smallest displacement can be obtained. However, the force acting on the slider in the tangential direction must be larger than the static friction level to ensure that a movement can be performed. The acceleration immediately after the slider moves depends mainly on the prestress, mass of the slider and the difference in the static and dynamic friction constants at the mating surfaces. Reducing the prestress or increasing the mass of the slider are not optimum approaches to reduce the acceleration. Since the actuation force of the vibrator suffers from the lack of adequate prestress, a light and slim construction with a small mass is desired. The remaining parameter is the difference in the static and dynamic friction constants, which depend on the tribological characteristics of the material. Altering the properties of the surface by lubrication or introducing a monolayer could be a possible solution [40]; however, the motor performance degrades when using this approach, and a continuous supply of lubrication is required due to the wearing of the mating surfaces. Therefore, in the following sections, a driving method is proposed to obtain a small motion and thus low velocities without changing the surface friction characteristics.

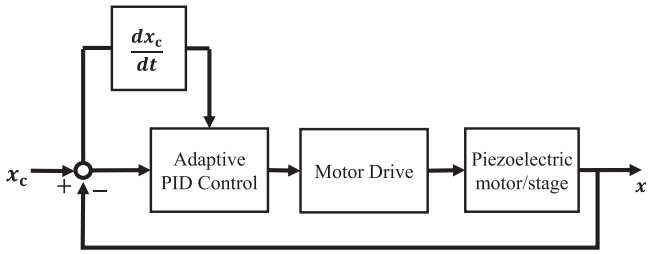

Fig. 3. Motion control loop.

C. Closed Loop Motion Control of RPM

A motion control algorithm is illustrated in Fig. 3. The input x_c is the commanded position, and output x is the actual position. The adaptive PID control algorithm uses the velocity information when making a decision for the next step. An inverse correlation exists between the velocity and PID parameter values.

The closed loop motion control of a piezoelectric motor system generally operates at a constant servo sampling frequency. After receiving the position information from the encoder, control algorithms such as the proportional–integral–derivative (PID) technique adjust the drive signal according to the tracking trajectory at the beginning of each servo period. The motor with the adjusted drive signal responds to the position change and reacts accordingly until the next feedback signal is received.

Since many of the piezoelectric motors operate at the resonance frequency ranging from 100 to 500 kHz, and most of the motion controllers have a servo sampling frequency of 10 to 20 kHz, in one servo sampling period of the digital motion controller, 5 to 25 pulses can occur at the operating frequency. When the first pulse exceeds the static friction force and causes the slider to move, the following pulses in the same servo sampling period make the slider move further until the next servo period. In this case, the amount of movement can be more than the commanded position. This problem affects the positioning accuracy of the slider severely, especially at velocities from 0.1 to 1.0 mm/s. Additionally, the nonlinear nature of friction can further aggravate the discontinuous movement. Fig. 4 shows a sample motor response to a commanded position at a velocity

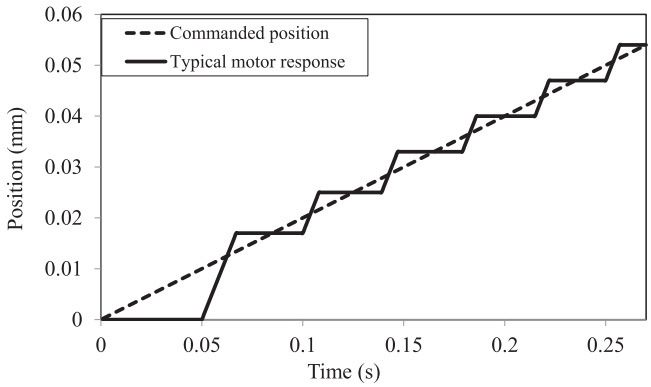

Fig. 4. Sample motor response and commanded position of a closed loop PID controller at a velocity of 0.2 mm/s.

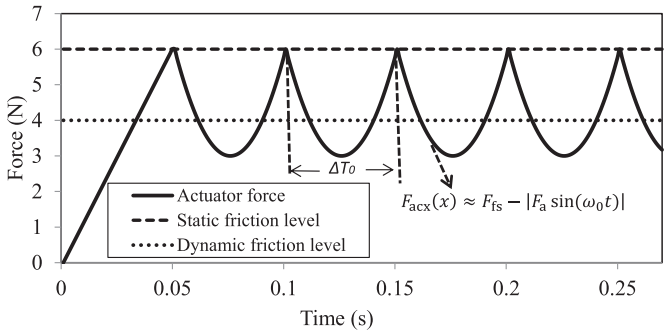

Fig. 5. Actuator force variation during closed loop operation with a velocity of 0.2 mm/s.

of 0.2 mm/s. The closed loop controller with a PID algorithm can only track the trajectory with zigzag movements. The commanded and actual measured positions are represented by dashed and solid lines, respectively.

When the force generated by the vibrator is larger than the static friction force level, the slider moves until the next servo command. If the actual position is higher than the commanded position, the magnitude of the driving voltage, and in turn, the force generated by the vibrator, reduce to less than the dynamic friction force level; therefore, the slider maintains its position. The corresponding vibrator force with the static and dynamic friction levels is simulated, as shown in Fig. 5, for a velocity of 0.2 mm/s. Assuming that the force generated by the vibrator is sinusoidal [41], the force acting on the slider can be expressed as follows:

$$F_{\text{acx}}(x) \approx F_{\text{fs}} - |F_a \sin(\omega_0 t)| \tag{10}$$

where F_{fs} is the static friction force level, and F_a is the difference between the force of the static friction and the minimum vibrator force during slow motion. The angular frequency ω_0 depends on the motor velocity, friction nonlinearity and PID parameters of the closed loop controller.

D. Friction Induced Forced Vibrations and Nature of Noise Generation at Slow Motion

A forced vibration or oscillation is caused by an external periodic force fed to the system. Such an oscillation mostly

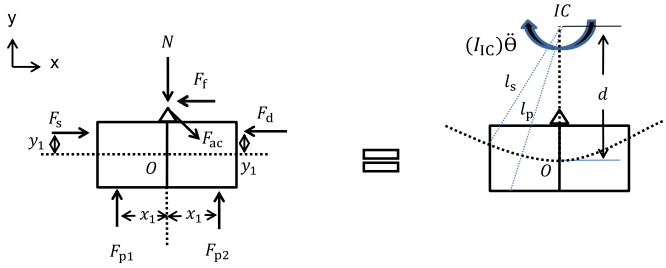

Fig. 6. Free body and kinetic diagram of the vibrator.

results in audible noise. The resonance drive type piezoelectric motor system can be modeled as a single degree of freedom forced vibration with viscous damping. Fig. 6 illustrates the free body diagram of the vibrator and corresponding kinetic diagram. In this model, the vibrator oscillates similar to a pendulum about the instantaneous center (*IC*) that has zero velocity.

Here, I_{IC} is the moment of inertia at the instantaneous center of zero velocity (*IC*) for the vibrator during the pendulum rotation, which depends on the mass and dimensions of the vibrator. As shown in Fig. 6, l_s, l_p, and d denote the distances from the *IC* to the location of the holder spring, prestress springs and center of gravity of the vibrator, respectively. The width of the piezoelectric vibrator is w. Assuming that the magnitude of the oscillatory movement θ is small, the following differential equation can be defined

$$\ddot{\theta} + \frac{2(F_s l_s + F_p l_p)}{I_{\text{IC}}}\theta + \frac{(F_{\text{acx}} - F_f)\left(d - \frac{w}{2}\right)}{I_{\text{IC}}} = 0 \tag{11}$$

Since damping leads to nonlinearities such as drift and hysteresis, the damping part is omitted in the abovementioned differential equation. Equation (11) is a second order linear differential equation for the rotational vibration of the piezoelectric element during slow motion. The natural frequency of the mechanical system, which depends on the static prestress, holding forces, geometry and moment of inertia, can be calculated as follows:

$$\omega_n = \sqrt{\frac{2(F_s l_s + F_p l_p)}{I_{\text{IC}}}} \tag{12}$$

By substituting the slider forces from (10) into (11), the differential equation can be written as

$$\ddot{\theta} + \frac{2(F_s l_s + F_p l_p)}{I_{\text{IC}}}\theta = \frac{(F_a)\left(d - \frac{w}{2}\right)|\sin(\omega_0 t)|}{I_{\text{IC}}}. \tag{13}$$

The general solution consists of a complementary solution $\theta_c(\text{t})$ and a particular solution $\theta_p(\text{t})$. The complementary solution is determined by setting the term on the right side of (13) to zero, and the effect is negligible. Since the motion is periodic, the particular solution of (13) can be determined by assuming a solution of the form

$$\theta_p(t) = A\sin(\omega_0 t) \tag{14}$$

where A is the amplitude of the angular oscillation from the forced vibration generated by the difference in friction between

the static and dynamic cases.

$$A = \frac{(F_a)\left(d - \frac{w}{2}\right)}{2(F_s l_s + F_p l_p)\left(1 - \left(\frac{\omega_0}{\omega_n}\right)^2\right)} \tag{15}$$

$$\theta_p\ (t) = \frac{(F_a)\left(d - \frac{w}{2}\right)}{2(F_s l_s + F_p l_p)\left(1 - \left(\frac{\omega_0}{\omega_n}\right)^2\right)} \sin(\omega_0 t)\,. \tag{16}$$

The amplitude of the forced vibration depends on the ratio of the frequencies ω_0/ω_n. The vibration amplitude increases as the frequency of the slider force (ω_0), which depends on the motor speed, friction nonlinearity, and the PID parameters, becomes closer to the natural frequency (ω_n) of the mechanical system.

The closed loop position controlled stages, which are driven at velocities between 0.001 mm/s and 1.0 mm/s, exhibit a friction induced forced vibration angular frequency that is close to the natural frequency of the motor. The angular frequency of the vibrator actuation force variation for a velocity of 0.2 mm/s and 0.6 mm/s has been calculated as approximately 150 rad/s and 350 rad/s, respectively. At such driving velocities, the amplitude of the force vibration increases drastically due to the ratio ω_0/ω_n. The increased vibration amplitudes result in the generation of audible noise at these velocities. The most critical factor is the velocity, which matches the natural angular frequency of the system. The natural angular frequency ω_n is approximately 413 rad/s; thus, the corresponding natural frequency f_n is 65.8 Hz, calculated using the piezoelectric material properties and geometrical parameters [36].

III. Driving Methods of RPM

A. Single Source Drive

The vibrator in the motor described in Section II.A has three electrical terminals. The electrode that covers one of the main surfaces completely is used as the common terminal, and the two other electrodes dividing the other main surface into two sections are the active terminals [35]–[37].

Driving the vibrator with one source means that a sine waveform is applied between one of the active and common terminals. The other active terminal is floating. At a specific aspect ratio between the length and width of the vibrator, a planar mode of the electrically driven section can be generated. With the geometry of the vibrator summarized in Table I, the planer mode, as shown in Fig. 7, occurs at approximately 153 kHz. This mode is the main resonance mode at which the motor operates. The impedance spectra shown in Fig. 12 corresponds to the free vibrator. When the vibrator is placed in the housing case due to the applied pressing and holding forces, the main operating frequency can increase up to 3 kHz. Fig. 7 shows that the surface area of the excited half expands and shrinks, while the unexcited half and pusher act as a perturbed mass. Since the pusher is attached at the center of the side surface, the tip of the pusher makes a back and forth movement in the oblique direction. The tip of the pusher, which is in contact with the slider, creates a pushing force. The direction of the slider movement can be changed with the driven electrodes.

TABLE I
Physical and Material Properties of the Vibrator

Quantity		Value
Length of piezo actuator	l	25 mm
Width of piezo actuator	w	11 mm
Distance from the center of gravity of the piezo actuator to the *IC*	d	12 mm
Mass of vibrator	m_v	0.009 kg
Spring force from the side	F_s	30 N
Prestress force	F_p	10 N
Dynamic friction constant	μ_d	0.2
Density	ρ	7800 kg/m^3

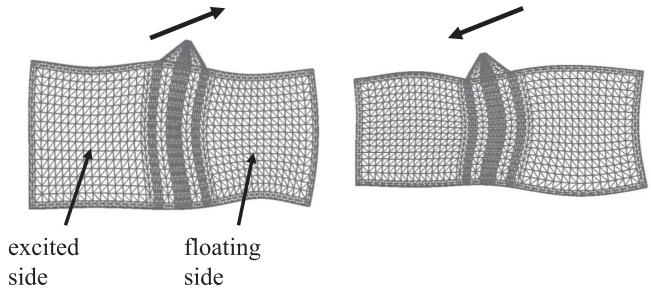

Fig. 7. Single source driving of the PILine motor in the resonance mode.

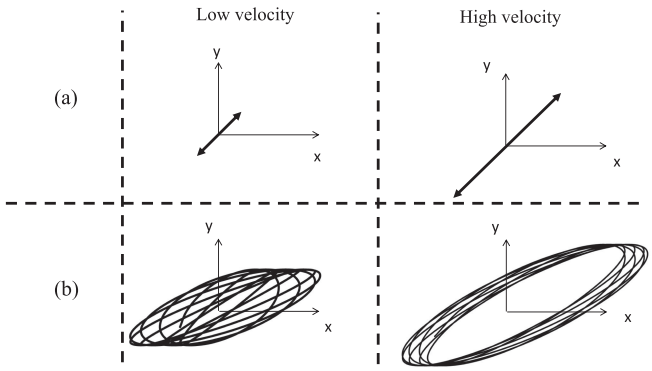

Fig. 8. Trajectories at the contact point of the friction tip. (a) Single source drive, the motion is in the oblique direction. (b) DSDF drive, the motion is a modulated ellipse changing in every cycle.

When the vibrator is driven with a single source, the motion on the pusher tip, as illustrated in Fig. 8(a), is in the oblique direction, and the forces generated by the vibrator in the x and y axis directions are almost equal [35]. At high speeds, such an oblique motion is ideal for obtaining a high performance. Every time the pusher applies a force onto the slider, the slider makes a microscopic movement. At low speeds, depending on the surface conditions, the oblique motion may not transfer sufficient force to the slider to realize a microscopic movement by exceeding the friction force. To induce a movement, the control electronic increases the driving voltage, thus increasing the magnitude of the oblique motion. Once the moving element performs a microscopic movement, the force between the friction tip and the slider reduces as the dynamic and static friction forces are

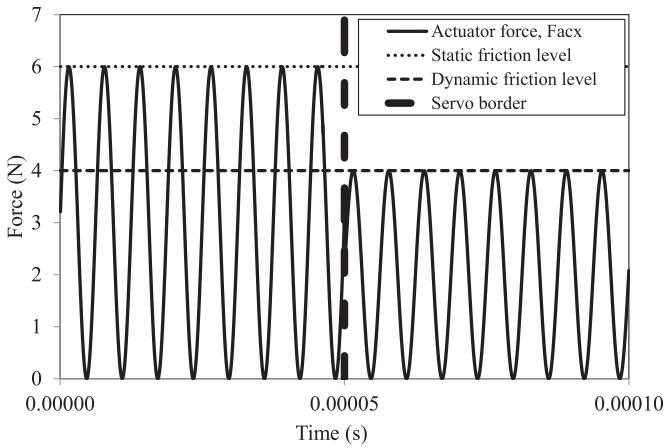

Fig. 9. Force in the x-axis direction for a single source drive type resonance piezoelectric motor. The frequency is the operating frequency of the motor, and the magnitudes are simulated using the parameters listed in Table I.

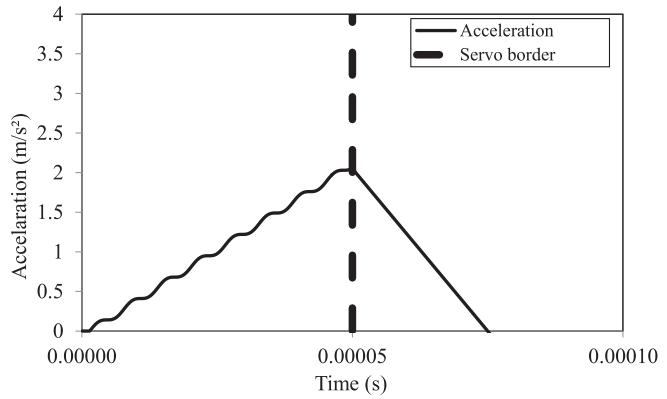

Fig. 10. Acceleration acting on the slider acted upon by the force of the stator.

different. This phenomenon results in a larger step or unpredictable movement of the slider, and this behavior is the main reason for the generation of the stick-slip motion, leading to the generation of audible noise at a low speed.

Fig. 9 shows the slider force in the x-axis direction within two servo cycles simulated by using the parameters presented in Table I. Since the servo sampling frequency is 20 kHz and operating frequency of the motor is 160 kHz, in one servo cycle, the vibrator pushes the slider 8 times. Due to the inertia of the slider, the acceleration increases in a stepwise manner in between two actuation force cycles (see Fig. 10). As expected, all of the control algorithms reduce the voltage amplitude in this case, thereby reducing the force of the actuator after the first servo cycle (1/20 kHz, 0.00005 s). When the force is reduced to less than the dynamic friction level, the deceleration commences, and the slider stops in the following servo cycle.

B. DSDF Driving of RPM

In the previous section, we described the difficulties and possible causes that prevent the realization of a smooth and slow movement in resonance drive type piezoelectric motors.

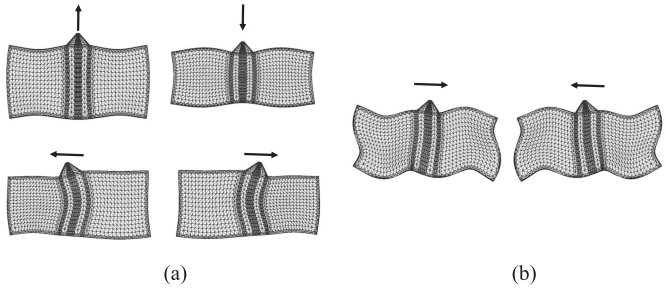

Fig. 11. Excited mode shapes when the motor is driven with a DSDF. (a) Two orthogonal resonance modes excited at the main resonance frequency (f1). (b) Resonance mode excited at the second frequency (f2).

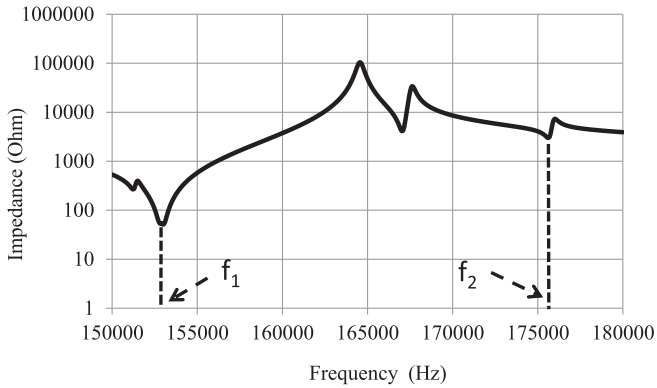

Fig. 12. Impedance spectrum of the piezoelectric vibrator. The friction tip performs an oblique or narrow elliptical movement at f_1. The tip performs a tangential back and forth movement at f_2.

In this section, we introduce a new driving method. When both the electrodes are electrically excited, the planar mode at the main operating frequency splits into two orthogonal resonance modes, as shown in Fig. 11(a). In this case, the pusher movement is elliptical. Even if the second excitation frequency (f_2) is approximately 20 kHz higher than the main operating frequency (f_1), the two orthogonal resonance modes are still excited at the main resonance frequency. The resonance mode around the second operating frequency, as shown in Fig. 11(b), is excited under the DSDF drive.

Note that the difference between the two driving frequencies is approximately 20 kHz, which is the frequency of the servo loop [39]. The second driving signal causes the friction tip to generate motion only in the tangential direction, and the displacement in the y-axis direction remains constant. The result is the modulated vibration trajectory of the friction tip, as shown in Fig. 8(b).

Driving the vibrator with two sources at two frequencies excites three resonance modes on the piezoelectric body. The first two modes are excited at the main operating frequency of the vibrator. As the frequency difference between f_1 and f_2 is synchronized to the closed loop servo frequency, the resulting slider force in the x-axis direction corresponds to the modulation of the two sinusoidal waveforms. The slider force obtained using the parameters listed in Table I was simulated, as shown in Fig. 13. Since the two driving signals are sinusoidal waveforms, and their phase differences are zero, the slider force exceeds the

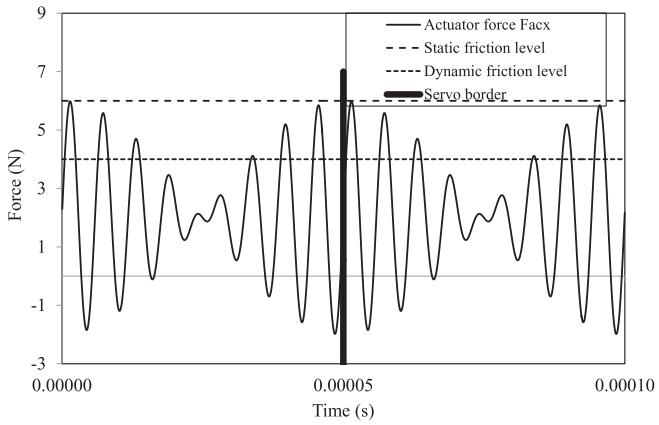

Fig. 13. Actuator force in the x direction for DSDF driving of a PUM.

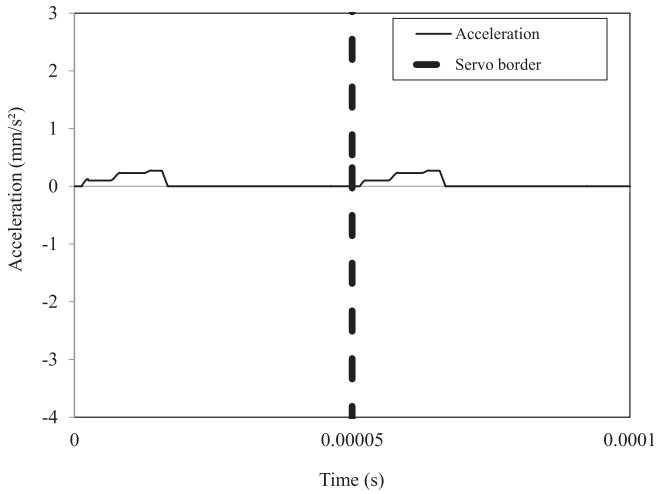

Fig. 14. Acceleration in two subsequent servo cycles for the DSDF driving of a PUM.

static friction force level as soon as the servo cycle begins. As the slider starts to perform a microscopic movement, the force starts to decrease due to the modulation of the force generated by the vibrator. The resulting acceleration acting on the slider increases in a stepwise manner until the force provided by the vibrator decreases under the dynamic friction level. Subsequently, the force transfer from the vibrator stops, as shown in Fig. 14. Compared to the single source drive case, the force applied by the slider is not present in the complete servo period. The resulting acceleration of the slider is smaller; consequently, the slider can make smaller steps, leading to lower velocities of the slider.

Using this driving method, a piezoelectric motor can be driven at a higher speed by reducing the voltage level of the second source. Reducing the voltage level of the second source makes the drive equivalent to a single source drive (see Figs. 15 and 16).

IV. Test Results

Fig. 17 shows the PILine system composed of an XY microscopy stage (U-781.NN) that includes two single axes linear stages oriented orthogonally on top of each other, a controller

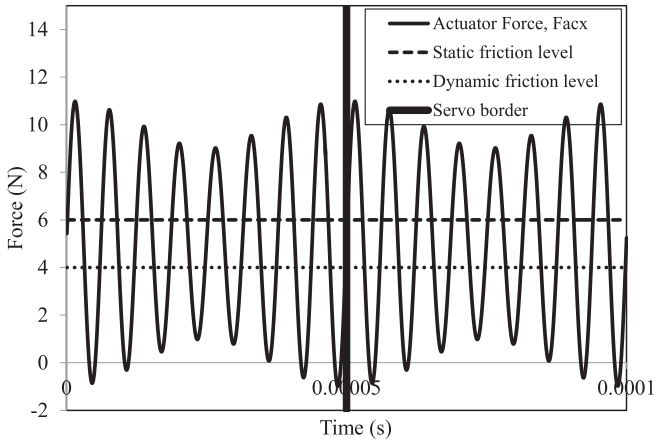

Fig. 15. High speed actuator force in the x direction for the DSDF driving of a PUM.

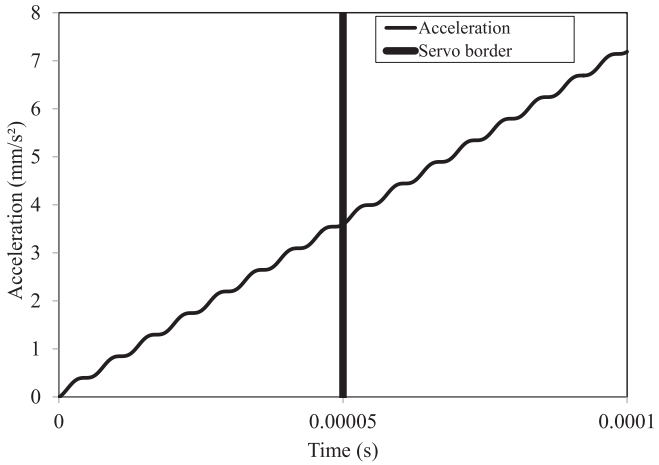

Fig. 16. High performance acceleration in two subsequent servo cycles for the DSDF driving of PUM.

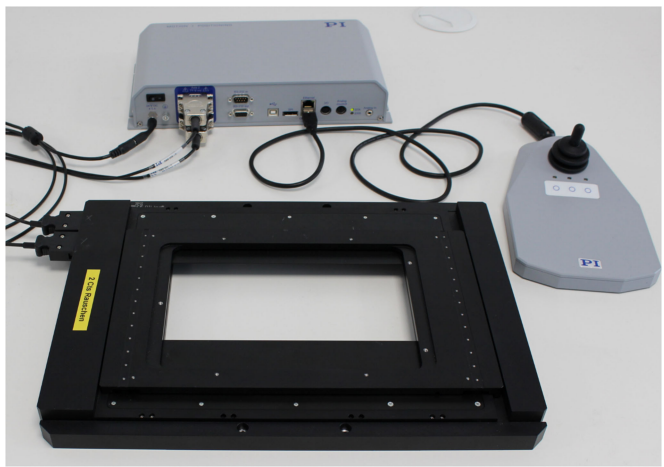

Fig. 17. Image of high resolution U-781.NN microscopy stage with a C-867.2U2 controller unit and joystick. The proposed driving method was embedded into the C-867.2U2 controller unit.

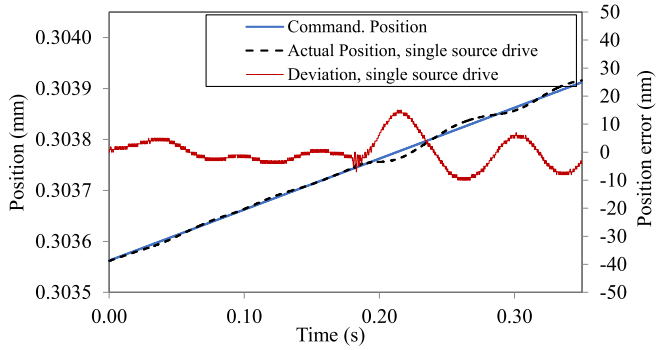

Fig. 18. Slow movement capability at 0.001 mm/s, and the position error between the commanded and actual positions for a single source drive.

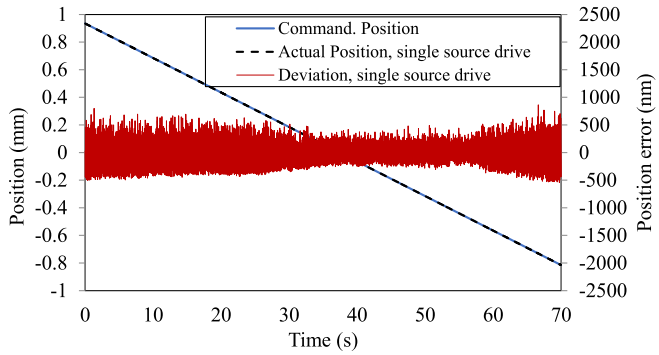

Fig. 19. Slow movement capability at 0.025 mm/s, and the position error between the commanded and actual positions for a single source drive.

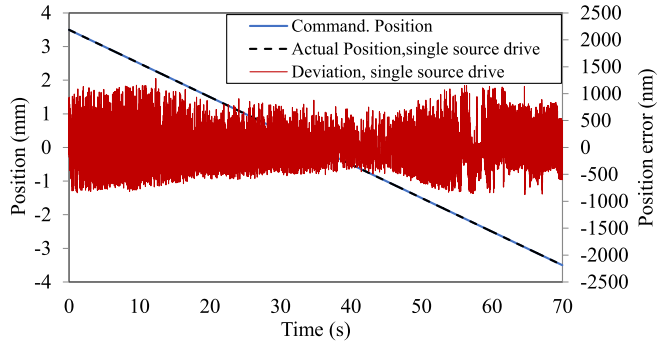

Fig. 20. Slow movement capability at 0.1 mm/s, and the position error between the commanded and actual positions for a single source drive.

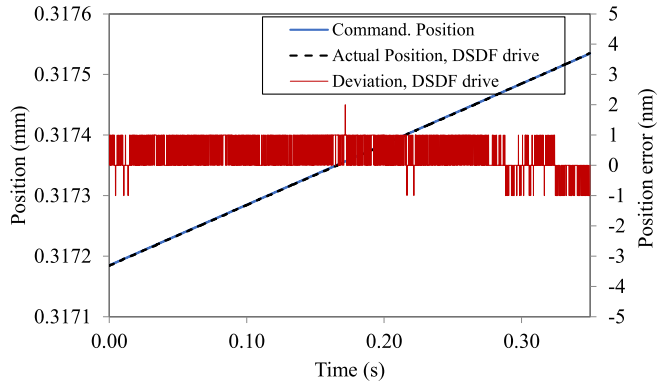

Fig. 21. Slow movement capability of the PILine stage with the DSDF drive at 0.001 mm/s, and the position error between the commanded and actual positions.

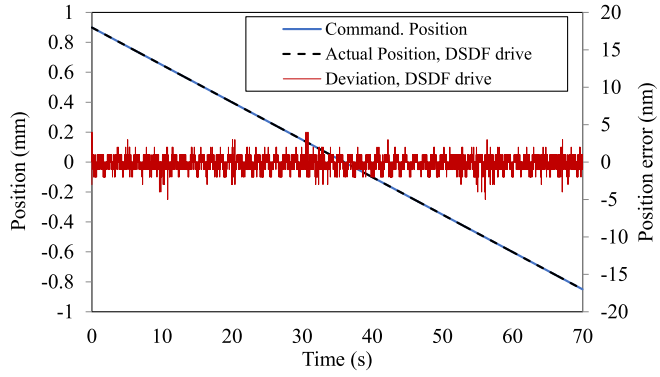

Fig. 22. Slow movement capability of the PILine stage with the DSDF drive at 0.025 mm/s, and the position error between the commanded and actual positions.

unit (C-867.2U2) and a joystick. The proposed driving method was tested on the high resolution microscopy stage. A noncontact optical incremental encoder (PIOne) integrated in this stage was used to measure the actual position directly at the motion platform with a high accuracy [44]. Even if the signal period of the encoder was 500 nm, the sensor interpolated resolution was reduced digitally to 1 nm, embedded in the controller. The measurements were performed under an ambient condition with a relative humidity of 60%. The stage had a travel range of 135 × 100 mm. The DSDF driving method with the relevant electronics was implemented in the controller.

First, the measurements for single source driving on both the X and Y moving axes of the microscopy stages were performed. As shown in Figs. 18 and 19, the magnitude of the deviations (position error) between the actual and commanded positions at speeds of 0.001 mm/s and 0.025 mm/s was approximately 20 nm and 500 nm for the bottom axes of the stage, respectively.

As shown in Fig. 20, the deviation at 0.1 mm/s was more than 1000 nm.

The same test was repeated for the DSDF drive to compare the deviations between the single source driving and DSDF driving. We used the same adaptive PID control for the single source drive. The position errors for the speeds of 0.001 mm/s, 0.025 mm/s, and 0.1 mm/s. are shown in Figs. 21–23. The deviations when using the proposed drive are one to two orders of magnitude less than those for the conventional single source drive for constant low velocities. Furthermore, the differences are large for the velocities of 0.025 mm/s and 0.1 mm/s (see Figs. 19–20 and 22–23). The movement at these low speeds when using the DSDF drive is smooth.

In addition to the linear movement at constant velocities, we evaluated the sinusoidal trajectory performance. The sinusoidal trajectories pertaining to two different frequencies generated and followed using the conventional single source and DSDF drive were obtained and illustrated in Figs. 24–27). The sine wave trajectories with amplitudes of 1.0 mm and 0.1 mm amplitudes were

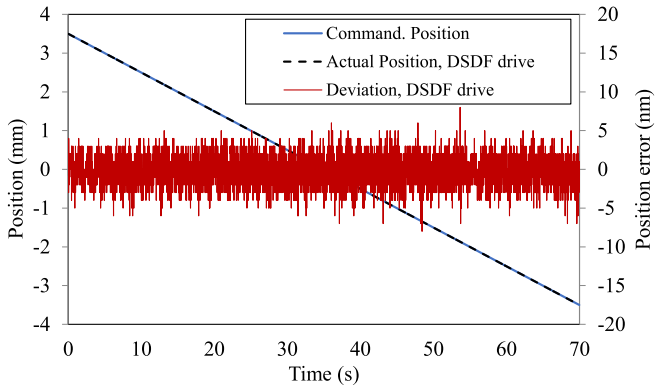

Fig. 23. Slow movement capability of the PILine stage with the DSDF drive at 0.1 mm/s and the position error between the commanded and actual positions.

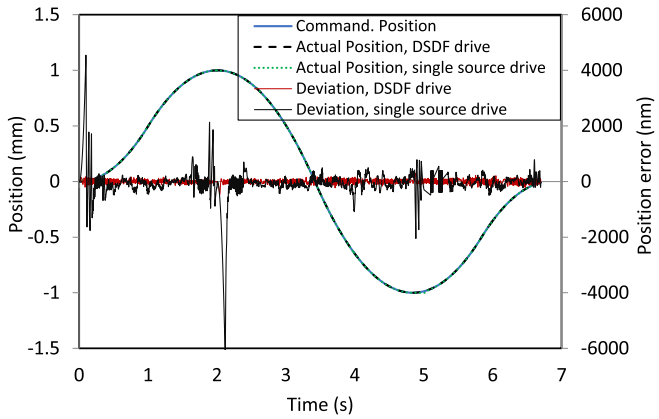

Fig. 24. Sine wave trajectory with an amplitude of 1 mm for single source and DSDF drives.

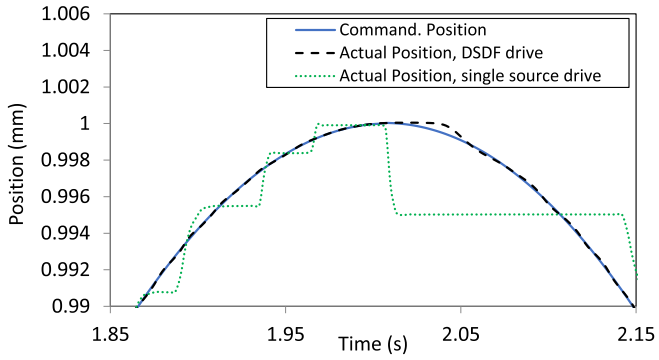

Fig. 25. Sine wave trajectory with an amplitude of 1 mm at the direction change for single source and DSDF drives.

generated and tested using a U-781.NN microscopy stage. It was noted that the conventional drive leads to a discontinuity in the trajectory following at low velocities when the direction changes due to the stick-slip nature of the contact friction between stator and slider of the piezoelectric motor. The same trajectories with the DSDF drives exhibit less tracking and contour position errors over the sine trajectories. The movement of the stage near the direction change is continuous, and less stick-slip nonlinearities are observed.

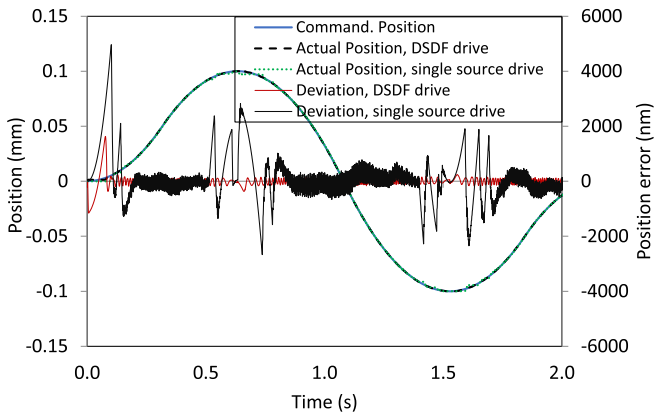

Fig. 26. Sine wave trajectory with an amplitude of 0.1 mm for single source and DSDF drives.

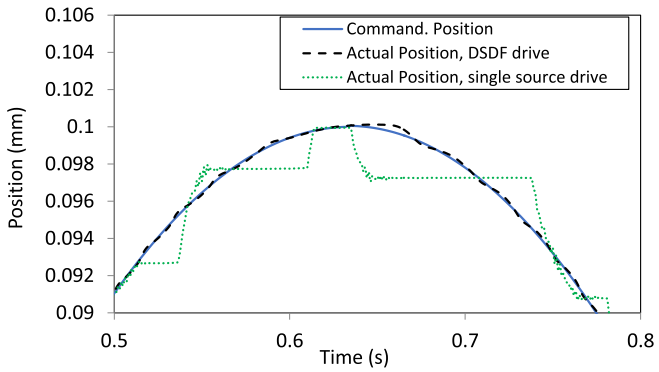

Fig. 27. Sine wave trajectory with an amplitude of 0.1 mm at the direction change for single source and DSDF drives.

As seen from Figs. 21 to 23, the position errors and deviations increase as the speed increases. The reason would be the friction condition mainly depends on the mated parts and friction also depends on the environmental conditions such as the temperature and humidity. However, as expressed in (16), the vibration amplitude is linearly related to F_a, which is the difference between the motor force in the moving direction ($F_{\rm acx}$) and friction force (F_f). By using the proposed driving method, F_a is minimized by controlling $F_{\rm acx}$. The change in the friction force F_f is compensated via adaptive PID control with the DSDF drive. However, the nonlinear friction changes cannot be completely controlled. The analytical model of slow motion for resonance drive type piezoelectric motors can be extended to other friction theories such as the Stribeck, LuGre, and Maxwell-slip models [9], [42], [43]. Additionally, the DSDF driving concept can be tested using sophisticated control methods for increasing the positioning accuracy and further reducing the velocity ripple during slow motion. The breakaway force remains the main obstacle to obtain linearized accurate motion, especially during circular trajectories, with two degrees of freedom x-y stage combinations. This driving concept can be combined with intelligent control algorithms to minimize the nonlinearities of the dead zone at the beginning of the motion.

V. Conclusion

In this article, a mechanical model, which describes the friction induced forced vibration and source of the noise generation in a resonance drive type piezoelectric motor was introduced. It was indicated that the closed loop controller parameters, such as the servo loop frequency and gain of the PID parameters to set the motor speed and friction nonlinearities are the sources of the friction induced vibrations. The amplitude of the friction induced vibration can disturb the slider movements, especially at low velocities, at which the frequency of the vibrator force during the closed loop operation and the frequency of the mechanical system are similar.

In a resonance drive type piezoelectric motor, the slider moving speed is controlled by the acceleration induced by the vibrator. When the resonance drive type piezoelectric motor is driven with one driving source, the force applied by the vibrator within one servo cycle is not controllable. Therefore, smooth constant movements cannot be realized, especially at low velocities.

To obtain a smooth movement at low speeds, a new driving method is proposed, in which the piezoelectric vibrator is excited with two driving sources at two different frequencies. In this driving method, the difference between the two excitation frequencies is synchronized to the closed loop servo sampling frequency of the digital controller. The microscopic motion of the friction tip at the interface is a modulated ellipse, which changes in every cycle. This type of microscopic motion reduces the acceleration of the slider; however, the force acting on the slider can exceed the breakaway friction force in every servo cycle. This phenomenon results in a silent and smooth movement, especially at a low velocity ranging from 0.001 to 1.0 mm/s. The test results indicate that the position error at these velocity ranges is less than 10 nm.

References

[1] B. Jaffe, J. W. Cook, and H. Jaffe, *Piezoelectric Ceramics*. London, U.K.: Academic, 1971.

[2] W. Chen and C. S. Lynch, "A micro-electro-mechanical model for polarization switching of ferroelectric materials," *Acta Mater.*, vol. 46, no. 15, pp. 5303–5311, Sep. 1998.

[3] K. Uchino, *Ferroelectric Devices*. New York, NY, USA: Marcel Dekker, 2000.

[4] K. Uchino, *Piezoelectric Actuators and Ultrasonic Motors*. Boston, MA, USA: Springer, 1996.

[5] B. Delibas and B. Koc, "L1B2 Piezo motor using D33 effect," in *Proc. 16th Int. Conf. New Actuators*, Actuator, Bremen, Jun. 2018, pp. 1–4.

[6] K. Spanner and B. Koc, "Piezoelectric motors, an Overview," *Actuators*, vol. 5, no. 1, pp. 6–18, Feb. 2016.

[7] C. Zhao, *Ultrasonic Motors, Technologies and Applications*. Berlin, Germany: Springer, 2011.

[8] T. Sashida and T. Kenjo, *Introduction to Ultrasonic Motors*. Oxford, U.K.: Oxford, 1993.

[9] C. Canudas de Wit *et al.*, "A new model for control of systems with friction," *IEEE Trans. Autom. Control*, vol. 40, no. 3, pp. 419–425, Jun. 1995.

[10] J. Wallaschek, "Contact mechanics of piezoelectric ultrasonic motors," *Smart Mater. Struct.*, vol. 7, no. 3, pp. 369–381, Jun. 1998.

[11] S.-C. Kim and S. H. Kim, "A precision linear actuator using piezoelectrically driven friction force," *Mechatronics*, vol. 11, no. 8, pp. 969–985, Dec. 2001.

[12] E. D. Tung, G. Anwar, and M. Tomizuka, "Low velocity friction compensation and feedforward solution based on repetitive control," *J. Dyn. Syst., Meas., Control*, vol. 115, no. 2A, pp. 279–284, Jun. 1993.

[13] J.-S. Mo *et al.*, "Adaptive positioning control of an ultrasonic linear motor system," *Rob. Comput. Integr. Manuf.*, vol. 44, pp. 156–173, Apr. 2017.

[14] S. Huang, W. Liang, and K. K. Tan, "Intelligent friction compensation: A Review," *IEEE/ASME Trans. Mechatronics*, vol. 24, no. 4, pp. 1763–1774, Aug. 2019.

[15] K. K. Tan and S. Huang, *Modeling and Control of Precision Actuators*. Boca Raton, FL, USA: CRC Press, 2017.

[16] G.-Y. Gu *et al.*, "Modeling and control of piezo-actuated nanopositioning stages: A Survey," *IEEE Trans. Autom. Sci. Eng.*, vol 13, no. 1, pp. 313–332, Jan. 2016.

[17] F. Kuang-Chao and L. Zi-Fa, "An intelligent nano-positioning control systems driven by an ultrasonic motor," *Int. J. Precis. Eng. Manuf.*, vol. 9, no. 3, pp. 40–45, Jul. 2008.

[18] E. Bekiroglu, "Ultrasonic motors: Their models, drives, controls and applications," *J. Electroceram.*, vol. 20, no. 3/4, pp. 277–286, Aug. 2008.

[19] T. Senjyu, T. Kashiwagi, and K. Uezato, "Position control of ultrasonic motors using MRAC with dead-zone compensation," *IEEE Trans. Ind. Electron.*, vol. 48, no. 6, pp. 1278–1285, Dec. 2001.

[20] Z. Jamaludin, H. Van Brussel, and J. Swevers, "Friction compensation of an XY feed table using friction-model-based feedforward and an inverse-model-based disturbance observer," *IEEE Trans. Indust. Electron.*, vol. 56, no. 10, pp. 3848–3853, Oct. 2009.

[21] F.-J. Lin *et al.*, "Recurrent fuzzy neural network control for piezoelectric ceramic linear ultrasonic motor drive," *IEEE Trans. Ultrason., Ferroelect., Freq. Control*, vol. 48, no. 4, pp. 900–913, Jul. 2001.

[22] T. Senjyu *et al.*, "Position control of ultrasonic motors using adaptive backstepping control and dead-zone compensation with fuzzy inference," in *Proc. IEEE Int. Conf. Ind. Technol.*, Bangkok, Dec. 2002, pp. 560–565.

[23] K. K. Tan, T. H. Lee, and H. X. Zhou, "Micro-positioning of linear-piezoelectric motors based on a learning nonlinear PID controller," *IEEE/ASME Trans. Mechatronics*, vol. 6, no. 4, pp. 428–436, Dec. 2001.

[24] Jian-Xin Xu and K. Abidi, "Discrete-time output integral sliding-mode control for a piezomotor-driven linear motion stage," *IEEE Trans. Ind. Electron.*, vol 55, no. 11, pp. 3917–3926, Nov. 2008.

[25] H. J. Pahk, D. S. Lee, and J. H. Park, "Ultra precision positioning system for servo motor–piezo actuator using the dual servo loop and digital filter implementation," *Int. J. Mach. Tools Manuf.*, vol. 41, no. 1, pp. 51–63, Jan. 2001.

[26] S. Ben-Yaakov, "Driver for piezoelectric motors," U.S. Patent 6 747 391 B1, Oct. 25, 1998.

[27] W. Liang *et al.*, "Control of a 2-DOF ultrasonic piezomotor stage for grommet insertion," *Mechatronics*, vol. 23, no. 8, pp. 1005–1013, Dec. 2013.

[28] MIL-STD-1474D, "Department of defense design criteria standard, Noise limits," Feb. 12, 1997.

[29] B. Armstrong-Helouvry, "Stick slip and control in low-speed motion," *IEEE Trans. Autom. Control*, vol 38, no. 10, pp. 1483–1496, Oct. 1993.

[30] R. A. Ibrahim, "Friction-induced vibration, chatter, squeal, and chaos—Part I: mechanics of contact and friction," *Appl. Mech. Rev.*, vol. 47, no. 7, pp. 209–226, Jul. 1994.

[31] R. A. Ibrahim, "Friction-induced vibration, chatter, squeal, and chaos—part II: dynamics and modeling," *Appl. Mech. Rev.*, vol. 47, no. 7, pp. 227–253, Jul. 1994.

[32] Yafei Pang *et al.*, "Performance evaluation of dual-frequency driving plate ultrasonic motor based on an analytical model," *IEEE Trans. Ultrason., Ferroelect., Freq. Control*, vol. 58, no. 8, pp. 1641–1650, Aug. 2011.

[33] Y. Ming *et al.*, "Performance improvement of rectangular-plate linear ultrasonic motors using dual-frequency drive," *IEEE Trans. Ultrason., Ferroelect., Freq. Control*, vol. 51, no. 12, pp. 1600–1606, Dec. 2004.

[34] M. Takano *et al.*, "Improvements in controllability of ultrasonic linear motors by longitudinal-bending multilayered transducers with independent electrodes," *Japanese J. Appl. Phys.*, vol. 50, no. 7, Jul. 2011, Art. no. 07HE25.

[35] O. Vyshnevskyy, S. Kovalev, and W. Wischnewskiy, "A novel, single-mode piezoceramic plate actuator for ultrasonic linear motors," *IEEE Trans. Ultrason., Ferroelect., Freq. Control*, vol. 52, no. 11, pp. 2047–2053, Nov. 2005.

[36] Physik Instrumente GmbH Co. & KG. [Online]. Available: https://www.physikinstrumente.com/en/. Accessed: Jul. 16, 2019.

[37] W. Wischnewsky and A. Wischnewsky, "Piezoelectric ultrasound motor," U.S. Patent 7 598 656 B2, Oct. 6, 2009.

[38] C. Stiebel *et al.*, "Method and device for actuating a piezoelectric motor," Int. Patent WO 2016091443 A1, Jun. 16, 2016.

[39] B. Delibas and B. Koc, "Method for closed-loop motion control of an ultrasonic motor," Eur. Patent E.P. 3435535 A1, Jan. 1, 2019.

[40] B. Bhushan, *Handbook of Nanotechnology*, 2nd ed., Berlin, Germany: Springer, 2007.
[41] T. Mashimo and K. Terashima, "Experimental verification of elliptical motion model in traveling wave ultrasonic motors," *IEEE/ASME Trans. Mechatronics*, vol. 20, no. 6, pp. 2699–2707, Dec. 2015.
[42] B. Amstrong-Hlouvry, "*Control of Machines with Friction*," Boston, MA, USA: Kluver Academic, 1991.
[43] J. Swevers, F. Al-Bender, C. Ganseman, and T. Prajago, "An integrated friction model structure with improved presliding behaviour for accurate friction compensation," *IEEE Trans. Autom. Control*, vol. 45, no. 4, pp. 675–686, Apr. 2000.
[44] Physik Instrumente GmbH Co. & KG. [Online]. Available: https://www.physikinstrumente.com/en/technology/sensor-technologies/pione-encoder/#c13864/. Accessed: Jul. 16, 2019.

Bülent Delibas received the Ph.D. degree in micromechanical model of piezoelectric materials from Mechanical Engineering Department, Kaiserslautern University of Technology, Kaiserslautern, Germany, in 2005.

He has been working as a Research and Development Engineer at PI (Physik Instrumente GmbH Co. & KG.), since 2006. He also teaches at Mechanical Engineering Department, Baden-Württemberg Cooperative State University (DHBW). His research interest include piezo motors, nonlinear control, smart structures, and precision stages.

Burhanettin Koc received the B.Sc. and M.Sc. degrees in electrical engineering from Hacettepe University, Ankara, Turkey, in 1989 and 1992, respectively, and the Ph.D. degree in piezoelectric actuators and motors from Electrical Engineering, Pennsylvania State University, PA, USA, in 1999.

He worked as an Assistant Professor at Mechatronics Engineering Department, Atilim University, Ankara, Turkey, from 2002 to 2004. From 2004 to 2008, he worked as Principal Researcher for Samsung Electro-Mechanics, S. Korea, involved in various miniaturized piezoelectric actuators and motors development projects for autofocus and zoom functions in cell phone cameras. He has been working as Senior Research and Development Engineer at PI (Physik Instrumente GmbH Co. & KG.), since 2008. He has more than 40 patents as an inventor or principal inventor and more than 30 publications in the area of piezoelectric actuators, motors and drive systems. His research interests include piezoelectric actuators and motors.